Protein Science (2000), *9*:2413–2426. Cambridge University Press. Printed in the USA.

Thermal stability of *Clostridium pasteurianum* rubredoxin: Deconvoluting the contributions of the metal site and the protein

FRANCESCO BONOMI,[1] DIMITRIOS FESSAS,[2] STEFANIA IAMETTI,[1] DONALD M. KURTZ, JR.,[3] AND STEFANIA MAZZINI[1]

[1]Dipartimento di Scienze Molecolari Agroalimentari, Università degli Studi di Milano, Via Celoria 2, I-20133 Milan, Italy
[2]Dipartimento di Scienze e Tecnologie Alimentari e Microbiologiche, Università degli Studi di Milano, Via Celoria 2, I-20133 Milan, Italy
[3]Department of Chemistry and Center for Metalloenzyme Studies, University of Georgia, Athens, Georgia 30602

(RECEIVED February 25, 2000; FINAL REVISION June 10, 2000; ACCEPTED September 22, 2000)

Abstract

To provide a framework for understanding the hyperthermostability of some rubredoxins, a comprehensive analysis of the thermally induced denaturation of rubredoxin (Rd) from the mesophile, *Clostridium pasteurianum* was undertaken. Rds with three different metals in its $M(SCys)_4$ site ($M = Fe^{3+/2+}$, Zn^{2+}, or Cd^{2+}) were examined. Kinetics of metal ion release were monitored anaerobically at several fixed temperatures between 40 and 100 °C, and during progressive heating of the iron-containing protein. Both methods gave a thermal stability of metal binding in the order $Fe^{2+} \ll Fe^{3+} < Zn^{2+} < Cd^{2+}$. The temperature at which half of the iron was released from the protein in temperature ramp experiments was 69 °C for Fe^{2+}Rd and 83 °C for Fe^{3+}Rd. Temperature-dependent changes in the protein structure were monitored by differential scanning calorimetry, tryptophan fluorescence, binding of a fluorescent hydrophobic probe, and ^{1}H NMR. Major but reversible structural changes, consisting of swelling of the hydrophobic core and opening of a loop region, were found to occur at temperatures (50–70 °C) much lower than those required for loss of the metal ion. For the three divalent metal ions, the results suggest that the onset of the reversible, lower-temperature structural changes is dependent on the size of the MS_4 site, whereas the final, irreversible loss of metal ion is dependent on the inherent M-SCys bond strength. In the case of Fe^{3+}Rd, stoichiometric Fe^{3+}/cysteine–ligand redox chemistry also occurs during metal ion loss. The results indicate that thermally induced unfolding of the native Cp Rd must surmount a significant kinetic barrier caused by stabilizing interactions both within the protein and within the $M(SCys)_4$ site.

Keywords: metal-derivatives; rubredoxin; thermal unfolding; thermostability

Rubredoxins (Rds) constitute a group of bacterial and archaeal iron–sulfur proteins of small size (~54 amino acid residues), containing a single, redox-active $Fe(SCys)_4$ site. The precise role of Rds in microbial physiology, especially in anaerobes, remains unclear, although evidence for an electron transfer function has been obtained (Gomes et al., 1997). All Rds contain the structural motifs shown in Figure 1 (Dauter et al., 1996), namely, two iron-coordinating CXXC loops (residues 6–9 and 39–42), a middle loop (residues 16–29), a three-stranded β-sheet involving both the N- and C-termini, and a hydrophobic core consisting of residues Y/W4, Y11, Y13, F30, I33, W37, and F49 (using *Clostridium pasteurianum* (Cp) Rd sequence numbering).

The issue of molecular determinants of thermostability in Rds arose upon the discovery of extremely thermostable Rds from hyperthermophiles, such as *Pyrococcus furiosus* (Pf) (Blake et al., 1991; Day et al., 1992; Hausinger et al., 1996). The secondary and tertiary structures of Pf Rd are nearly superimposable on those of the mesophilic Cp Rd. Introduction of the three-stranded β-sheet sequence of Pf Rd into Cp Rd did not confer Pf Rd-like thermostability (Richie et al., 1996; Eidsness et al., 1997; Bau et al., 1998). Cavagnero et al. have reported that thermally induced unfolding of Cp Fe^{3+}Rd is monophasic at pH 2, whereas that of Pf Fe^{3+}Rd is multiphasic (Cavagnero et al., 1998a, 1998b). Hiller et al. found that the peptide NHs involved in N—H—S(Cys) hydrogen bonds of the $Zn(SCys)_4$ site in zinc-substituted Pf Rd were the most thermally stable to exchange with solvent protons (Hiller et al., 1997).

Reprint requests to: F. Bonomi, DISMA, Via Celoria 2, 20133 Milan, Italy; e-mail: francesco.bonomi@unimi.it.

Abbreviations: ANS, 1-anilinonaphthalene-8-sulfonate, sodium salt; BPS, bathophenanthroline sulfonate, sodium salt; CD, circular dichroism; DSC, differential scanning calorimetry; FeRd, iron-containing rubredoxin; ICP-AE, inductively coupled plasma-atomic emission; Rd, recombinant rubredoxin from *Clostridium pasteurianum*; TCA, trichloroacetic acid; Tris, tris(hydroxymethyl)aminomethane; Zn(Cd)Rd, zinc-(cadmium)-containing rubredoxin.

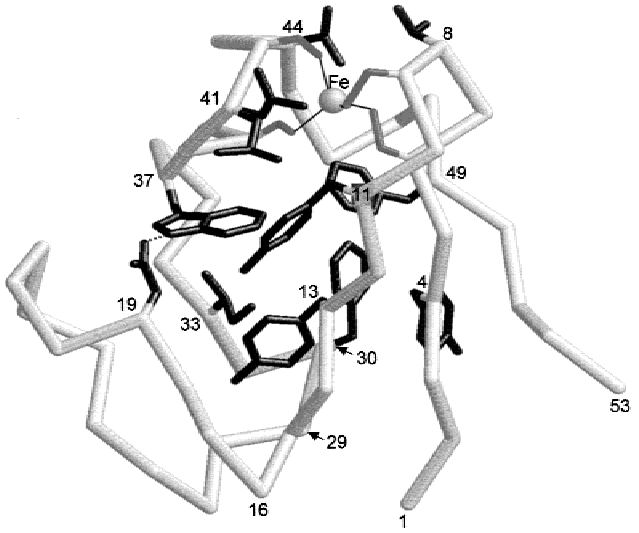

Fig. 1. A diagram of the structure of Cp FeRd. The protein α-carbon backbone is represented in lighter shade. The three-stranded β-sheet is on the right, the two CXXC-containing loops are at the top, and the middle loop is to the lower left. Several pertinent side chains are portrayed as wire frame in the darker shade. Several sequence positions along the backbone are labeled near their alpha carbons. Thin lines connecting the sphere represent cysteine sulfur ligation to the iron atom. Dashed line represents a hydrogen bond between the carboxylate of D19 and indole NH of W37. The side chain of L41 has two rotamers in the crystal structure. The drawings were generated with RASMOL (Sayle & Milner-White, 1995) using coordinates in file 1IRO deposited in the Protein Data Bank (Dauter et al., 1996).

In all of the aforementioned studies, the thermally induced denaturation of the Rds was irreversible. A recent report has shown that a metal-free mutant of Pf Rd, in which all ligand cysteine residues were mutated, unfolds reversibly with a T_m of 82 °C (Strop & Mayo, 1999), whereas an analogously mutated mesophilic Rd remained unfolded even at 1 °C. These results indicate that the metal site is the source of the irreversibility observed upon thermal unfolding of Rds, but that it is not the source of the hyperthermostability of Pf Rd.

Although iron is the only known native metal ion in Rd, ZnRd is the major product of overexpression of Cp Rd in *Escherichia coli* (Richie et al., 1996). Recently we showed that both Cd^{2+} and Zn^{2+} can directly displace Fe^{2+} from Rd in buffer at neutral pH and room temperature in vitro without resorting to protein denaturation (Bonomi et al., 1998). Direct quantitative displacement of Zn^{2+} by Cd^{2+} was also shown for ZnRd upon incubation with a modest excess of cadmium salts. This displacement order is consistent with the expected trend in thiophilicity of these divalent metal ions, i.e., $Cd^{2+} > Zn^{2+} > Fe^{2+}$ (Werth & Johnson, 1990; Pountney & Vasak, 1992; Brouwer, 1996; Bonomi et al., 1998). The crystal structure of Cp ZnRd is nearly superimposable on that of the Cp FeRd (Dauter et al., 1996). X-ray crystallographic (Dauter et al., 1996) and ^{1}H-NMR studies (Richie et al., 1996; Eidsness et al., 1997; Bertini et al., 1998) of Cp MRds (M = Fe, Zn, or Cd) showed a significant expansion of the $M(SCys)_4$ coordination sphere for M = Cd (Ayhan et al., 1996) vs. Zn or Fe, and other localized rearrangements of side chains. Nondenaturing Cd^{2+} displacement of Zn^{2+} in Cp Rd was found to occur without "unzipping" of the β-sheet (Bonomi et al., 1998). Thus, mostly local adjustments are made to accommodate the larger $Cd(SCys)_4$ site in Cp Rd without significantly affecting overall protein structure or decreasing overall protein stability at room temperature.

To provide a basis for understanding the nature of the hyperthermostabilizing interactions in Pf Rd, we have attempted in this work to define, characterize, and deconvolute the various steps in thermal denaturation of the structurally very similar, but mesophilic, Cp Rd near pH 7. Among the issues addressed are: (1) the contribution of $M(SCys)_4$ site stability to the protein's thermal stability, (2) detection of partially unfolded forms of the protein, (3) specific contributions of defined regions of the protein to thermostability, (4) solvent exposure of the hydrophobic core during heating, (5) redox chemistry occurring upon Fe^{3+} release, and (6) the sequence of and relative kinetic barriers to processes (1)–(5).

Results

Thermal stability of the $M(SCys)_4$ site

All of the experiments described below were conducted under anaerobic conditions in aqueous solutions buffered with 50 mM Tris-HCl, pH 7.4. No correction was made for the temperature-dependent pH of Tris buffer. Prolonged heating of the Cp MRds, where M = $Fe^{2+,3+}$, Zn^{2+}, or Cd^{2+}, at temperatures higher than 70–90 °C resulted in the release of significant amounts of metal ion from the $M(SCys)_4$ sites at appreciable rates. Less than 10% of the metal was released after 3 h incubation of ZnRd at 70 °C and of CdRd at 80 °C. As shown in Figure 2, the proportion of metal ion released from the MRds under comparable time and temperature combinations at neutral pH and in the absence of chelating agents follows the order $Fe^{2+} \gg Fe^{3+} > Zn^{2+} > Cd^{2+}$. The much lower thermostability of the $M(SCys)_4$ site for M = Fe^{2+} in Cp Rd correlates with our previous results from metal displacement experiments carried out at room temperature (Bonomi et al., 1998). Identical results were obtained using either dithionite-reduced FeRd

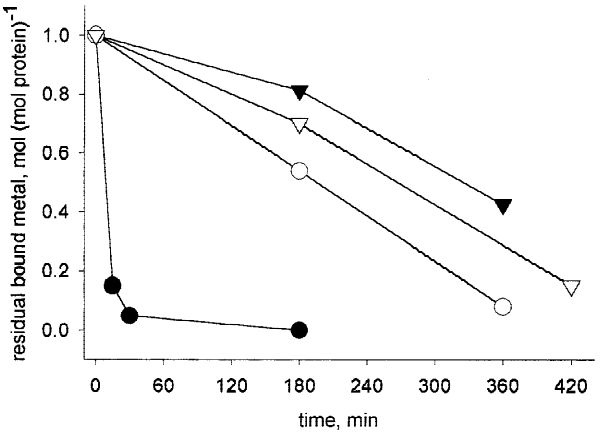

Fig. 2. Time course of metal ion release from MRds at 90 °C. Rd solutions (0.02 mM in 50 mM Tris-HCl, pH 7.4) were heated anaerobically at 90 °C. For M = Fe^{2+}, sodium dithionite was added to 2 mM prior to heating. Aliquots were withdrawn at the times indicated by the data points, diluted into cold buffer, and exhaustively buffer-exchanged in Centricon® devices. Residual metal content in the retentate (protein-bound metal) was determined by ICP-AE spectrometry. Full circles, Fe^{2+}; full triangles, Cd^{2+}; open triangles, Zn^{2+}; open circles, Fe^{3+}.

or FeRd, which had been photoreduced in the presence of 1 μM deazaflavin (not shown), thus ruling out any direct effect of dithionite on Fe^{2+} release. We previously observed that reduction of the Fe^{3+} to Fe^{2+} in FeRd was required for its displacement by either Cd^{2+} or Zn^{2+} at room temperature (Bonomi et al., 1998). We attributed this requirement to the lower thiophilicity of Fe^{2+} relative to Fe^{3+}. However, from the trend in thermally induced metal ion loss shown listed above, it might be inferred that Fe^{3+} has a lower affinity for Rd than does Cd^{2+} or Zn^{2+}. As demonstrated below, the source of this seeming discrepancy is reduction of Fe^{3+} upon its thermally induced release from oxidized Cp Rd.

A more detailed study of the thermally induced denaturation of the $Fe(SCys)_4$ site was carried out for the two redox forms of FeRd. For oxidized FeRd, the characteristic visible absorption feature of the native $Fe^{3+}(SCys)_4$ site at 492 nm was used to follow the time course of its destruction at various temperatures, as shown in Figure 3. No significant thermal perturbation of the characteristic UV-Vis absorption spectrum of oxidized Cp FeRd, other than its progressive loss of intensity was evident in these experiments, confirming previous observations (Eidsness et al., 1997). These observations rule out the occurrence of any significant structural alterations in the oxidized $Fe(SCys)_4$ site prior to either its reduction or metal ion loss.

Most of the time courses shown in Figure 3 were found to follow quite closely pseudo-first-order kinetics, although evidences for a multiphasic behavior were evident at temperatures between 80 and 90°C, where several concomitant phenomena may occur (vide infra).

Because there is no easily monitored absorbance in the colorless solutions of the reduced Cp FeRd, we resorted to chelating the released Fe^{2+} with BPS, as in our previous kinetic studies on metal substitution (Bonomi et al., 1998). The temperature-dependent release of iron in the presence of BPS was also monitored for the oxidized Cp FeRd. An approximation of the relative thermal stability of the native Fe^{2+} vs. Fe^{3+} metal sites in Rd is represented by the results from temperature ramp experiments presented in Figure 4. In these experiments, release of iron was monitored continuously while progressively increasing the temperature of

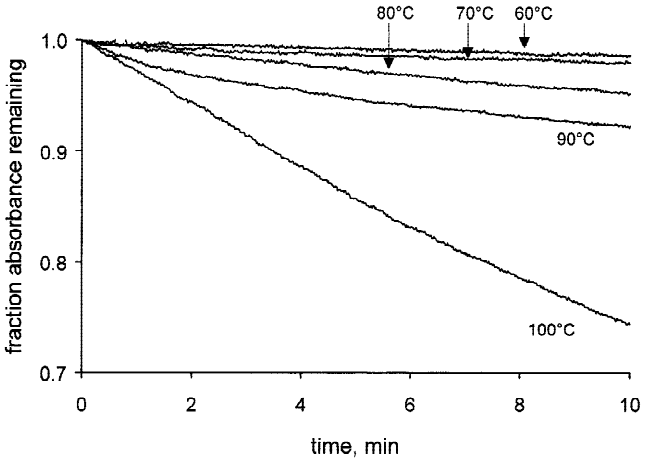

Fig. 3. Time course of absorbance changes during heating of Cp Fe^{3+}Rd. The protein (0.01–0.02 mM in 50 mM Tris-HCl, pH 7.4) was incubated at the various temperatures (in °C) indicated next to each curve while continuously monitoring the absorbance at 492 nm.

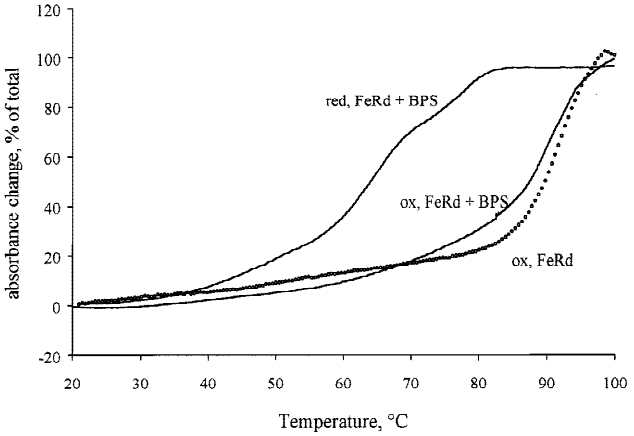

Fig. 4. Absorbance changes upon progressive heating of oxidized and reduced FeRd. FeRd (0.01–0.02 mM in 50 mM Tris-HCl, pH 7.4) was heated progressively from 20 to 100 °C at heating rate of 0.5 °C/min. When appropriate, the protein was reduced with 5 mM dithionite. When present, BPS was 0.2 mM. Absorbance changes were monitored at either 535 nm (reduced + BPS and oxidized + BPS), or at 492 nm (oxidized, dashed line).

the Rd solutions at the fixed rate of 0.5 °C min^{-1}. These temperature ramp experiments confirm the lower thermal stability of the $Fe(SCys)_4$ site in reduced vs. oxidized FeRd. In the case of oxidized FeRd, the nearly coincidental temperature-dependent loss of A_{492} and formation of the colored Fe^{2+}(BPS) complex at 535 nm confirms the absence of a direct role of BPS in iron release. This coincidence also means that Fe^{3+} must be rapidly reduced upon its release from the oxidized Rd, because Fe^{3+} does not form a red-colored complex with BPS. From these experiments, it is also possible to estimate a midpoint temperature for the thermally induced metal ion release (T_m). Taking into account the kinetic factors determined in the experiments presented below and the heating rate (Riva & Schiraldi, 1993), we estimated T_m to be 69 °C for the reduced FeRd and 83 °C for the oxidized FeRd.

The temperature dependence of iron release from Cp Rd in either oxidation state and in the presence of BPS are compared in the Arrhenius plots of Figure 1S, where—for the sake of simplicity—all the spectroscopic changes were fitted to apparent pseudo-first-order kinetics. We found no appreciable difference between rate constants for loss of iron from the oxidized FeRd in the presence of BPS, measured by monitoring formation of the Fe^{2+}–BPS complex, vs. the absence of BPS, measured as a decrease in A_{492}. Within the limitations inherent to the simplification of this kinetic analysis, no appreciable difference is evident between the Arrhenius activation energies measured for iron release from oxidized FeRd in the presence (72 kJ mol^{-1}) or absence of BPS (70 kJ mol^{-1}). This observation confirms that, under anaerobic conditions, the thermally induced absorbance decrease for oxidized Cp FeRd (Fig. 3), which measures $Fe^{3+}(SCys)_4$ site destruction, is accompanied by rapid release of Fe^{2+} from the protein, and that BPS does not actively remove iron from Rds even at elevated temperatures. The relative lability of the iron in reduced Rd is also confirmed by its Arrhenius plot, which shows a marked transition temperature at 57 °C. Below this temperature, the estimated E_a for Fe^{2+} release is the same measured for the oxidized protein (i.e., 70 kJ mol^{-1}), but increases to 250 kJ mol^{-1} at higher temperature.

Table 1. *Residual metal content and titratable thiols in Cp MRds heated at 90 °C for different times*

Rd	Heating time (h)	Residual metal (moles/mol protein)	Titratable –SH[a] (moles/mol protein)
Fe, reduced	3	0.03 ± 0.02	3.82 ± 0.23
Fe, oxidized	None	1.02 ± 0.06	0.08 ± 0.04
	3	0.61 ± 0.05	1.15 ± 0.34
	8	0.02 ± 0.01	2.91 ± 0.11
Cd	3	0.82 ± 0.13	0.62 ± 0.11
	8	0.22 ± 0.07	3.22 ± 0.18
Zn	3	0.70 ± 0.08	1.22 ± 0.14
	8	0.11 ± 0.11	3.82 ± 0.21
Acid-prepared apoprotein	None	0.02 ± 0.01	4.06 ± 0.18

[a]Titratable –SH was determined using Ellman's chemistry (Ellman, 1959), in the absence of denaturants. Residual metal content in Rd was determined by ICP-AE after Centricon® dialysis to remove unbound metal ion. Average values and standard deviation are for three separate experiments. Apo-Rd was prepared by precipitating the native FeRd with 10% TCA, followed by two washes of the precipitate with 1% TCA and redissolution in buffer.

Free thiol and metal content after heating MRds

Free –SH content in the Cp MRds was correlated with metal content after heating. The only cysteine residues in Cp Rd are the four that provide ligands to the metal ion. The results listed in Table 1 show that four free –SH per mol of Rd were determined after removal of the metal ion upon prolonged anaerobic heating of Cd-, Zn- or dithionite-reduced FeRd. This free thiol/protein stoichiometry rules out decomposition of cysteine to dehydroalanine or oxidation of thiols during thermally induced M^{2+} release under our anaerobic conditions. At lower temperatures and/or shorter heating times, the proportion of reactive thiols was consistent with four thiols becoming accessible for each divalent metal ion lost. In the case of oxidized FeRd, when the protein was heated anaerobically long enough to induce complete loss of iron, we found three rather than four reactive thiols in the residual protein. The most obvious explanation for these results is formation of a disulfide via reduction of Fe^{3+} upon heating of oxidized Rd. No evidence for polymeric forms of Rd was found in gel-permeation experiments carried out on oxidized FeRd after prolonged heating and complete metal ion loss, arguing against intermolecular disulfide formation (and against any other type of heat-induced protein aggregation).

Differential scanning calorimetry of Cp MRds

DSC, in principle, can directly measure heat capacity changes associated with conformational transitions. The DSC tracings obtained in anaerobic conditions for three of the four Cp MRds investigated in this study are presented in Figure 5. The dithionite-reduced FeRd did not show any appreciable DSC signal at temperatures below those where thermal decomposition of dithionite interferes with the measurements (~80 °C). None of the MRds showed the sharp endothermic peak typical of a cooperative thermal transition between native and denatured states of a compact globular protein (Privalov, 1979). Instead, we observed only a modification in the heat capacity (ΔCp), which could be interpreted as due to an increased hydration of protein residues and/or to an increased conformational freedom in the unfolded protein (Sturtevant, 1977; Privalov, 1979; Privalov & Gill, 1989; Privalov & Makhatadze, 1993; Barone et al., 1994).

Despite the nonstandard shapes of the DSC curves, it is clear that the temperatures required for the DSC transitions do not correlate with those obtained from the metal ion release experiments discussed above. Oxidized FeRd apparently undergoes conformational changes at the lowest transition temperature (52 ± 1 °C) and with the lowest change in specific heat capacity (ΔCp = 8 ± 2 $J\,K^{-1}\,mol^{-1}$). This transition temperature is far below that at which half-release of iron occurs (83 °C) under comparable heating conditions (cf. Fig. 4). CdRd shows a DSC transition at a temperature significantly lower (72 ± 1 °C) than that observed for ZnRd (94 ± 1 °C), but with a larger change in heat capacity (CdRd = 19 ± 2 $J\,K^{-1}\,mol^{-1}$; ZnRd = 14 ± 2 $J\,K^{-1}\,mol^{-1}$). The midpoint temperatures for all the transitions observed in DSC are considerably below those expected assuming that metal release is the event corresponding to (or responsible for) unfolding of the protein. The overall $\Delta_d Cp$ (T_d) effect, expressed in $J\,K^{-1}\,mol^{-1}$ per aminoacid residue, is 160 in Fe^{3+}Rd, 250 in ZnRd, and 357 in CdRd. Estimates of $\Delta_d Cp$ (T_d) for other proteins are in the range of 50–110 $J\,K^{-1}\,mol^{-1}$ per aminoacid residue (Privalov & Makhatadze, 1990),

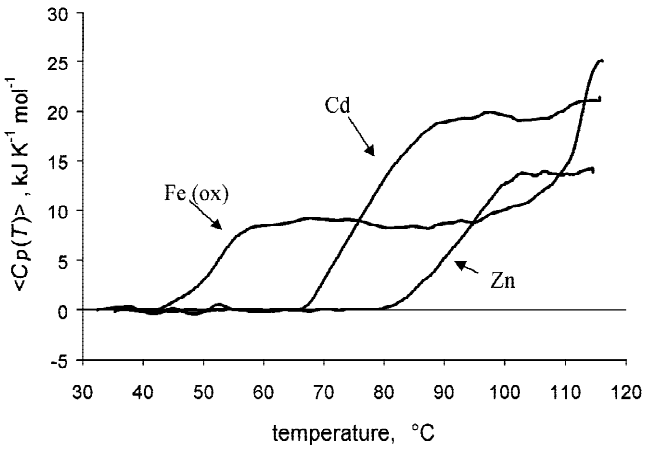

Fig. 5. DSC tracings for Cp MRds. Rd solutions (0.4–0.5 mM in 50 mM Tris-HCl, pH 7.4) were heated progressively at 0.5 °C/min.

a portion of which was attributed to changes in the water-accessible surface area upon unfolding, and the remainder to increased conformational freedom of the protein in the unfolded state. The relative contribution of the two effects is reportedly dependent on the nature and size of the protein (Privalov & Makhatadze, 1992). Apparently, the nature of the metal ion in the $M(SCys)_4$ site affects the changes in residue solvation and/or in interconversion among conformers upon heating.

In a separate experiment, oxidized FeRd was heated to 60 °C under the DSC conditions (that is, enough to undergo the transition reported in Fig. 5, but well below the temperature required for significant iron release) and then rapidly cooled to 20 °C. This temperature-cycled protein showed the same transition near 52 °C when re-analyzed by DSC, and retained almost completely the UV/Vis absorption features and intensities of the starting protein. These observations indicate that the lower temperature structural transitions of Fe^{3+}Rd observed by DSC are reversible, and not accompanied by significant metal ion release.

ANS binding to heated MRds

To assess whether the thermally induced structural changes and metal ion release corresponded to exposure of hydrophobic regions of the protein structure, the Cp MRds were heated in the presence of the fluorescent hydrophobic probe, ANS (Ptitsyn, 1992; Cairoli et al., 1994). Changes in the intensity of ANS fluorescence stem from its binding to sufficiently exposed hydrophobic regions in proteins. Due to overlap of the ANS emission maximum (480 nm) with one of the absorbance maxima (492 nm) of oxidized FeRd, and of the ANS excitation wavelength (390 nm) with the near-UV absorption of dithionite, these experiments were limited to the Cd and ZnRds. Fluorescence spectra of ANS in the presence of Cd or ZnRds obtained at 20 °C and at 90 °C (Fig. 2S in Supplementary material in the Electronic Appendix) indicate a small but significant increase in ANS fluorescence over background, which is attributed to binding of the probe to newly exposed hydrophobic regions on the protein surface. These changes were not observed when heating mixtures of ANS and apoRd. The change in ANS fluorescence during temperature ramp experiments carried out on mixtures of either Cd or ZnRd and ANS under the same conditions as used for metal ion release studies, is plotted in Figure 6.

The tracings in Figure 6 clearly indicate temperature-dependent exposure of hydrophobic regions at a lower temperature for CdRd than for ZnRd. The midpoint temperatures of the ANS transitions observed for the Cd and ZnRds (~50 and ~60 °C, respectively) were far below those required for significant release of metal ion (70 and 80 °C, respectively), and were also lower than the temperatures at which DSC-detectable transitions occurred (cf. Fig. 5).

Tryptophan fluorescence of heated MRds

W37 is the only Trp residue in Cp Rd and is located in a well-defined hydrophobic core (cf. Fig. 1). Tryptophan fluorescence studies were, therefore, carried out to assess the involvement of this region of Rd in the lower temperature transitions observed by DSC and ANS fluorescence. Due to interfering background absorption of dithionite, we did not carry out these experiments on reduced FeRd. Trp fluorescence spectra recorded for ZnRd, CdRd, and Fe^{3+}Rd at 20 °C, at 100 °C, and after cooling back to 20 °C are shown in the appropriate panels of Figure 7. No modifications in the position of the Trp emission maximum, which would indicate

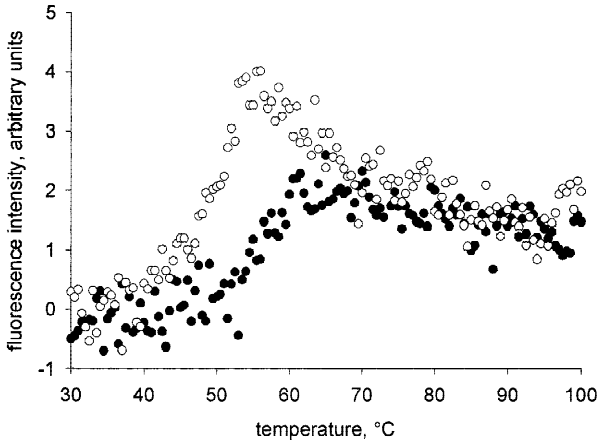

Fig. 6. Fluorescence intensity changes upon progressive heating of mixtures of ANS and CdRd (open symbols) or ZnRd (full symbols). Rd solutions (0.01 mM in 50 mM Tris-HCl, pH 7.4, containing 0.1 mM ANS) were heated progressively from 20 to 100 °C at a rate of 0.5 °C/min. Fluorescence at λ_{em} = 480 nm was monitored continuously by using λ_{ex} = 390 nm. The experimental tracings are corrected for the background increase in fluorescence in heated ANS solutions.

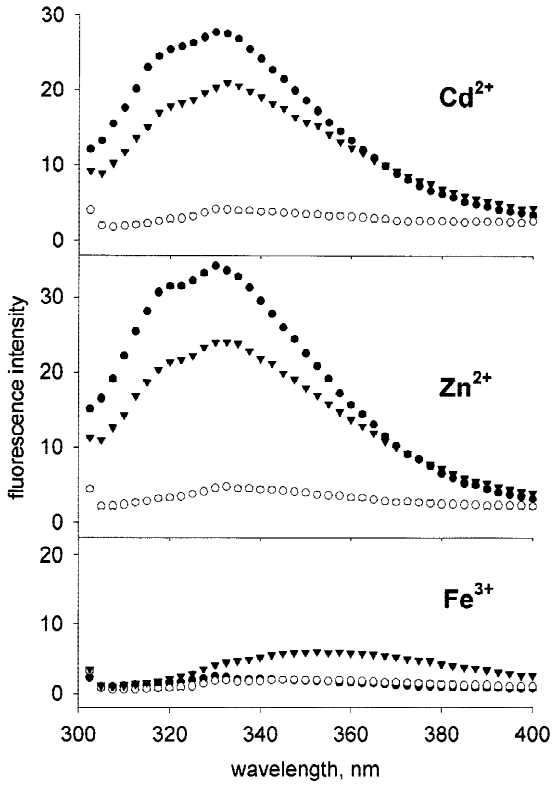

Fig. 7. Effects of temperature on the W37 fluorescence spectra of Cp MRds. Rds (5–8 μM in 50 mM Tris-HCl, pH 7.4) were heated progressively from 20 to 100 °C at a rate of 0.5 °C/min, and kept at 100 °C for 5 min before being re-cooled to 20 °C at 10 °C/min. Shown are the emission spectra (λ_{ex} = 298 nm) of the untreated protein at 20 °C (full circles), the protein at 100 °C (open circles), and the protein after re-cooling to 20 °C (triangles). Spectra obtained at intermediate temperatures are omitted for clarity.

a change in solvent exposure, were evident in spectra taken at 5 °C intervals (not shown) during heating of Zn and CdRd, but there was an evident, temperature-dependent decrease of the fluorescence intensity. As shown in Figure 7, most of this intensity decrease in ZnRd and CdRd could be reversed upon cooling back to 20 °C, consistent with recovery of a native-like structure in that portion of the protein that did not undergo irreversible modifications as a consequence of metal ion release.

In the case of the oxidized FeRd, a combination of the protein absorbance and the quenching effect of iron resulted in a very low quantum yield for W37, and did not allow monitoring of temperature-dependent changes in fluorescence other than a modest intensity increase (Fig. 7) associated with iron release (Cavagnero et al., 1998b).

Under the conditions of these experiments (that included a 10 min incubation at 100 °C at the end of a 20–100 °C temperature ramp in 160 min), an appreciable fraction of the iron was lost from the oxidized FeRd (cf. Figs. 2, 3; Table 1). After the residual protein was cooled, its W37 fluorescence emission spectrum showed a significantly red-shifted maximum (Fig. 7) likely as a consequence of some exposure of the indole ring to solvent. The red-shifted emission maximum of this "displaced" W37 was the only signal present in the emission spectrum of an iron-depleted Rd obtained by heat treatment of the oxidized FeRd, and was much less pronounced in the spectra of metal-depleted Rds obtained by prolonged heating of Cd and ZnRd, or in the spectra of an apoprotein obtained by TCA precipitation of oxidized FeRd (Fig. 3S in Supplementary materials in the Electronic Appendix). This comparison suggests that the W37 environment is considerably different in the heat-treated oxidized FeRd than in the other heated MRds.

The emission intensities of the W37 fluorescence in Cd and ZnRd during the temperature ramp experiments decreased continuously with increasing temperature (above 30 °C), and no intermediate transitions were evident (Fig. 4S in Supplementary materials in the Electronic Appendix). These data indicate that, in Cd and ZnRd, the reversible changes of the W37 fluorescence intensity monitor only modifications in the contacts between the exposed edge of the indole ring and surrounding molecules (including solvent), but not changes in contacts involving the indole ring faces, as made evident by the absence of shifts in the emission maximum (Fig. 7).

Far-UV CD spectroscopy of heated MRds

Far-UV CD spectroscopy indicated essentially complete loss of secondary structure when Cd or ZnRd were heated long enough to result in complete metal ion release. The heated apoproteins had a much lower content of residual secondary structure than a Rd apoprotein obtained by TCA treatment at room temperature (Fig. 8).

^{1}H NMR of heated MRds

To provide more detailed information about the structural regions of Cp Rd that are involved in these thermally induced changes, the temperature dependences of selected resonances in the ^{1}H NMR spectra of MRds was monitored. Due to paramagnetic broadening of resonances for Fe^{3+}Rd, the experiments were limited to the Rds containing Fe^{2+}, Zn^{2+}, and Cd^{2+}, the vast majority of whose ^{1}H NMR resonances have been assigned (Richie et al., 1996; Eidsness et al., 1997; Bertini et al., 1998; Bonomi et al., 1998). As shown in the three panels of Figure 9, several resonances are displaced or

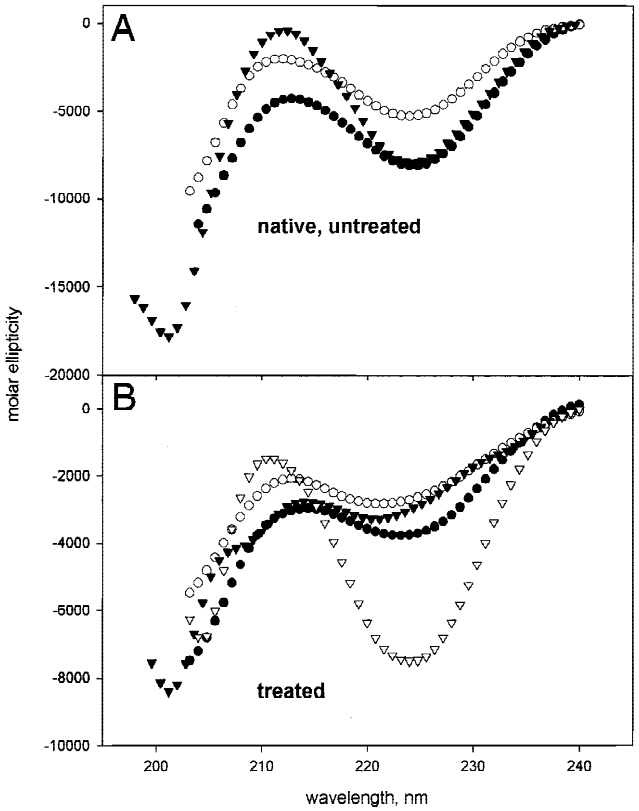

Fig. 8. Far-UV CD spectra of Fe^{3+}Rd (full triangles), ZnRd (open circles), and CdRd (full circles), (**A**) before and (**B**) after treatment at 90 °C for 8 h. The spectrum of Cp apoRd obtained as described in the footnote to Table 1 by TCA precipitation of Fe^{3+}Rd (open triangles) is shown in the lower panel for comparison. Proteins were ~10 μM in 50 mM Tris-HCl pH 7.4. Spectra were taken at 25 °C in 1 mm pathlength cells.

reduced in intensity when the temperature is raised. In the cases of Zn and CdRd, most of the distinguishing spectral features disappear at 80 °C, but are almost fully recovered, both in position and in intensity, upon re-cooling to 25 °C. This recovery indicates that nearly all of the thermally induced structural modifications that occur without metal ion release, are reversible.

Particularly notable are the well-resolved resonances of two side chains in the hydrophobic core, namely, the indole ring NH of W37 (at 11.55 ppm for CdRd at room temperature) and the δCH_3 of I33 (at −1.17 ppm for CdRd at room temperature). The latter upfield resonance position is most likely due to a ring current effect from the nearby W37 indole side chain (cf. Fig. 1). The positions of these two resonances as a function of temperature are plotted in Figure 10. The W37 indole NH resonance shifts at a somewhat lower temperature in CdRd than in ZnRd, and completely disappears at temperatures above 65 °C in CdRd or above 75 °C in ZnRd. In contrast, the indole NH resonance is still present at 80 °C in the spectrum of reduced FeRd. The disappearance of this resonance probably occurs concomitantly with breakage of a hydrogen bond between the W37 indole NH and a carboxylate oxygen of the side chain of D19, thereby allowing the indole NH proton to exchange with solvent. The upfield shift of the I33 δCH_3 with increasing temperature shows an almost perfect overlap in the case of Zn and CdRd, including the change in slope at ~65 °C. A much

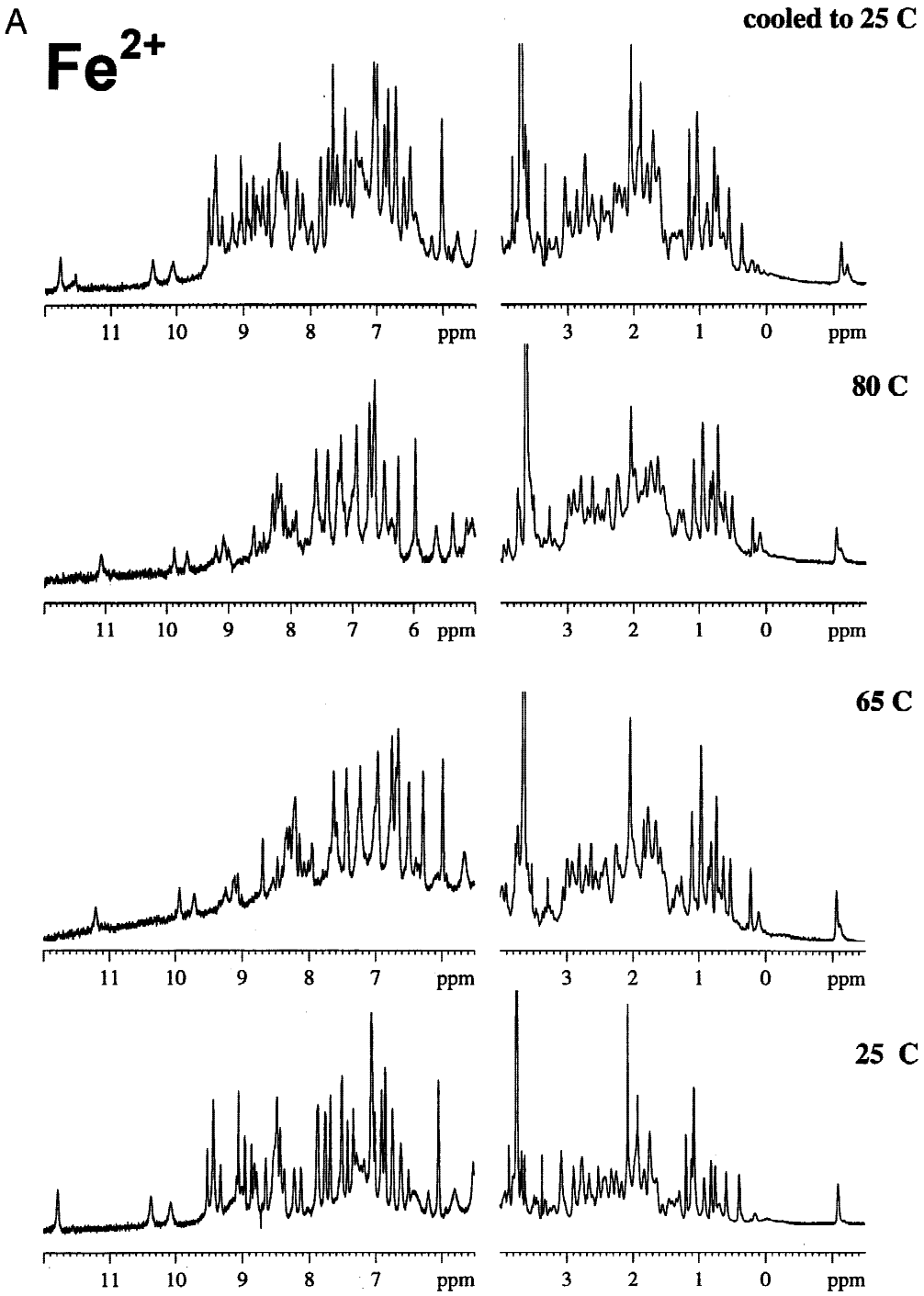

Fig. 9. ^{1}H-NMR spectra of Cp MRds at various temperatures. Spectra were taken on anaerobic solutions of 0.2–0.6 mM Rd in 5 mM Tris-HCl, pH 7.4, containing 10% D_2O (v/v) and 5 mM sodium dithionite in the case of reduced FeRd. Spectra were obtained at 5 °C intervals during progressive heating to 80 °C and after re-cooling to 25 °C. Heating rate was ~1 °C/min. At each preset temperature, about 5 min were allowed for thermal equilibration of the sample prior to spectral acquisition, which required 15–20 min for each preset temperature. (*Figure continues on facing pages.*)

shallower temperature dependence of the I33 δCH_3 resonance is observed upon heating reduced FeRd. The relatively smooth and monotonic temperature dependence of these resonances is most likely due to rapid (on the NMR timescale) fluctuations among an ensemble of protein conformers ranging from native to largely unfolded but with the $M(SCys)_4$ site intact.

In the Cd and ZnRd, a detailed analysis of the spectral region of aliphatic side chains between 0 and 1.5 ppm indicates that resonances attributable to residues V8 and L41 as well as to V44 undergo small but significant shifts with temperature (0.03–0.05 ppm from 25 to 65 °C, as exemplified in Fig. 11 for CdRd). The aforementioned side chains lie close to the $M(SCys)_4$ site (cf. Fig. 1). In

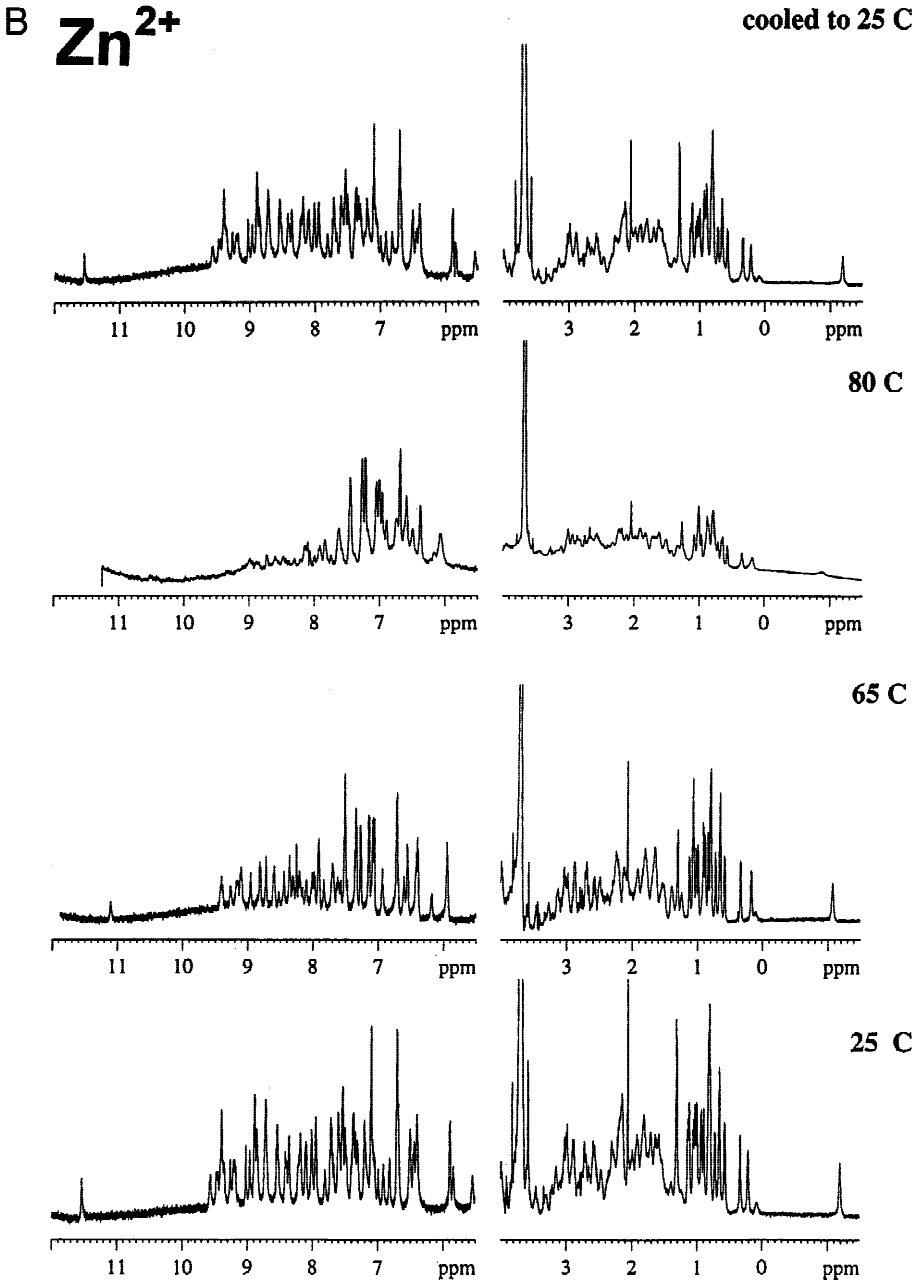

Fig. 9. *Continues.*

the Cd- and ZnRds, only very modest temperature-dependent shifts are observed for resonances of aliphatic residues located in other regions of the protein, such as I12 and L52 on the middle and C-terminal strands, respectively, of the β-sheet. Residual paramagnetism prevented accurate measurements in this region for Fe^{2+}Rd. Other resonances, in particular those of the backbone amide NHs, almost completely disappear at high temperature (see the 80 °C spectra in Fig. 9) indicating extensive breakage of hydrogen bonds.

When the NMR data are compared with those obtained by the other methods, it appears that the transitions detectable by DSC in Zn and CdRd occur only after complete exposure of the W37 indole ring edge to solvent and approximately coincide with the onset of the I33-δCH_3 NMR disappearance (presumably due to its shifting to a position within the group of methyl resonances downfield of 0 ppm).

Discussion

The most pertinent data obtained in this work for the thermal modifications of Cp MRds are collected in Table 2. The results show that: (1) thermally induced "spontaneous" metal ion release from MRds occurs during the last and irreversible step of protein unfolding; (2) thermally induced metal ion release occurs in the order: $Fe^{2+} \gg Fe^{3+} > Cd^{2+} > Zn^{2+}$; (3) the committed step in release of iron from oxidized FeRd appears to be reduction of Fe^{3+} to Fe^{2+} and a corresponding 1:1 stoichiometric oxidation of cys-

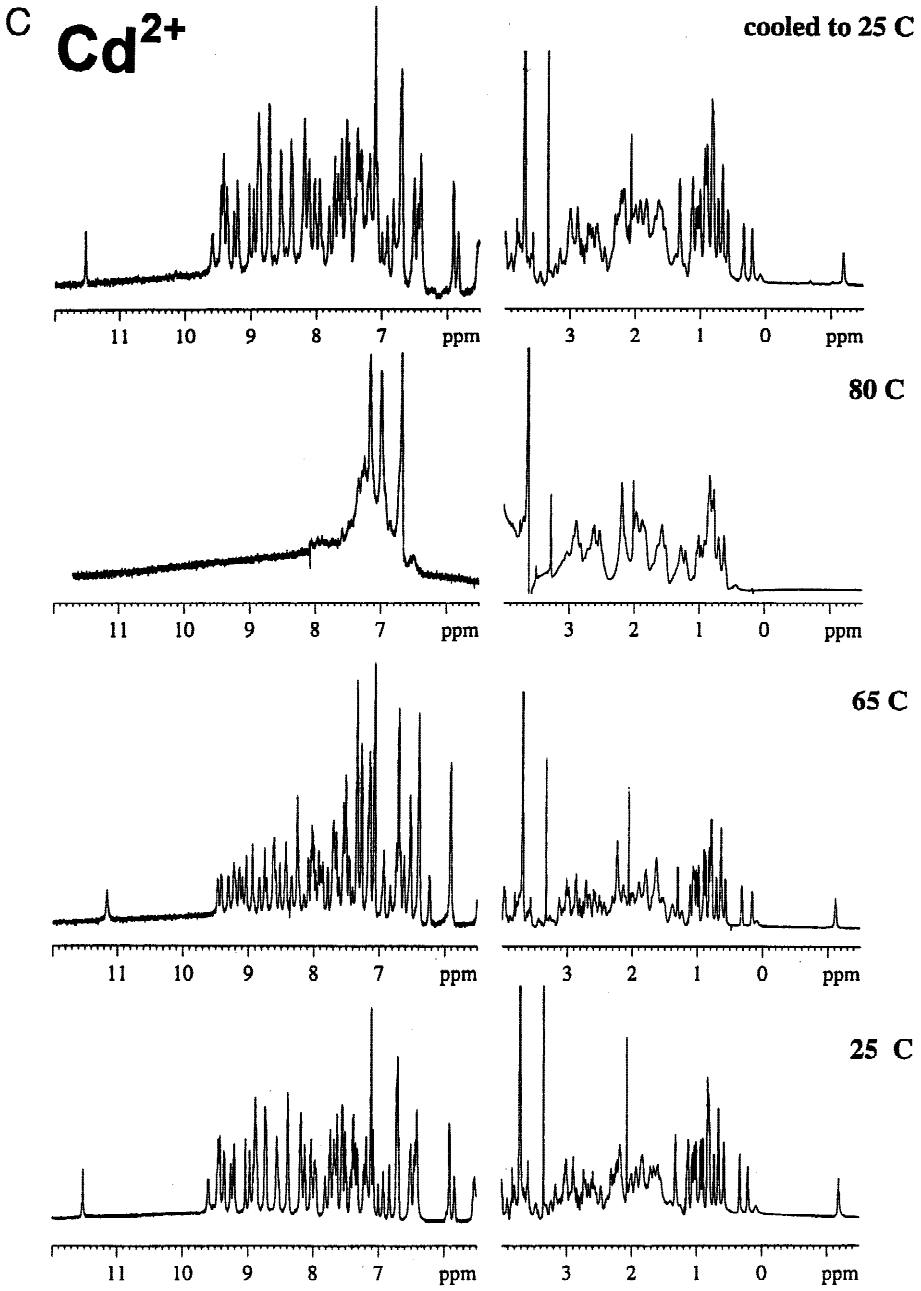

Fig. 9. *Continued.*

teine thiols, but no protein aggregation; (4) at temperatures below those required for metal ion release, structural modifications occur in the hydrophobic core and middle loop regions but not at the $M(SCys)_4$ sites; (5) modifications of the protein structure occur at lower temperature for CdRd than for ZnRd; (6) the acid-prepared Cp apoRd does retain a large amount of secondary structure at room temperature, whereas heat-prepared apoRds do not.

We interpret our results in a model for the thermal unfolding process and subsequent metal ion loss in Fe^{2+}, Cd, and ZnRds (i.e., in those Rds where no redox chemistry of the metal ion is possible under anaerobic conditions) shown in Scheme 1. In this scheme, reversible protein structural modifications and the irreversible events resulting in metal ion release occur in clearly distinct temperature regimes.

The first event, occurring when temperature is increased, is interpreted as a progressive "loosening" or "swelling" of the hydrophobic core of Rd, which includes W37 as a convenient marker of structural integrity. Although this residue likely retains its original orientation with respect to other nearby residues, major progressive changes are observed in the spectroscopic (fluorescence, NMR) properties of W37.

These changes are reversible and do not detectably affect other regions of the protein. As the temperature is raised above a definite threshold (~50 °C for CdRd and ~60 °C for ZnRd), temperature-

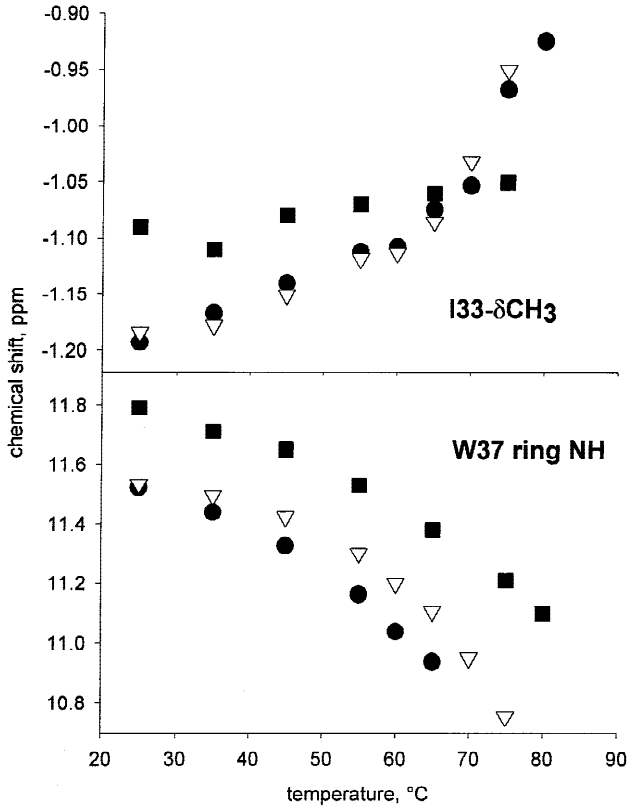

Fig. 10. Temperature dependence of the I33-δCH_3 and the W37 indole ring NH resonances in the ^{1}H NMR spectra of Cp MRds. Circles, CdRd; triangles, ZnRd; squares, reduced FeRd.

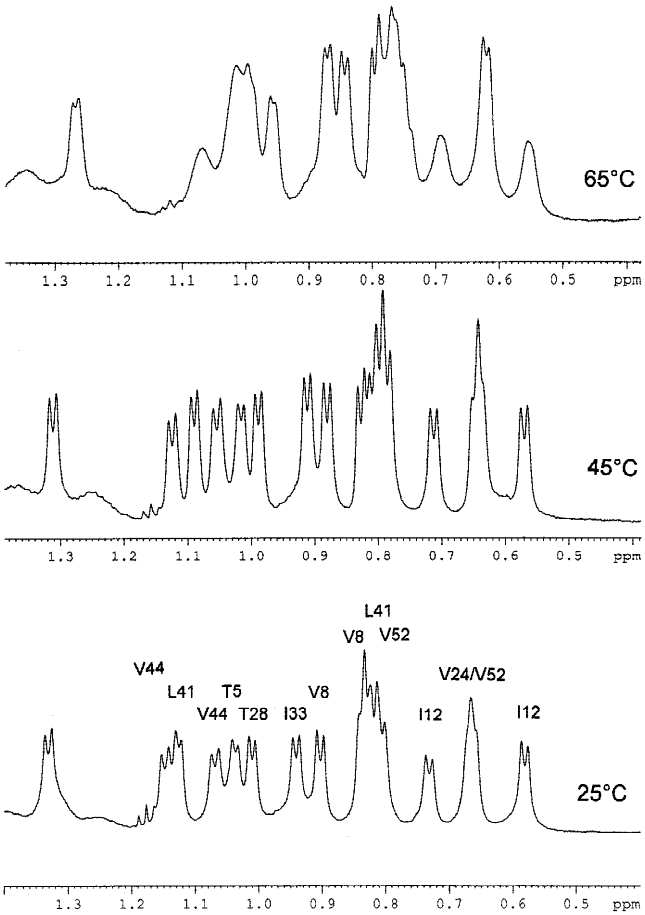

Fig. 11. Aliphatic region of the ^{1}H-NMR spectra of Cp CdRd at the given temperatures. Resonances at 25 °C were assigned according to Bonomi et al. (1998).

induced modifications become more extensive and apparently involve other regions of the protein in addition to the hydrophobic core. The temperature-dependent changes in ^{1}H NMR chemical shifts of both I33 δCH_3 and the W37 indole ring NH become steeper, and this latter signal eventually disappears, due to solvent exposure. The solvent exposure of the W37 indole NH is likely due to breakage of a hydrogen bond to the D19 carboxylate in the middle loop. As a result, this loop may move away from the hydrophobic core, thereby exposing the core to solvent. Previously buried regions of the protein do indeed become solvent-exposed in this temperature regime, as shown by DSC and by binding of the ANS probe. The change in fluorescence intensity upon heating the mixture of Rd and ANS is modest, as expected for such a small protein (Ptitsyn, 1992) and is consistent with formation of hydrophobic patches having a limited surface and with the lack of aggregation during heating observed by gel permeation (Iametti et al., 1996, 1998). Breakage of the W37 indole NH/D19-carboxylate hydrogen bond had been predicted by molecular dynamics simulations of thermal unfolding pathways for oxidized FeRds (Lazaridis et al., 1997). In fact, our proposed progression of unfolding events is remarkably similar to that obtained from these molecular dynamics simulations, which treated the Fe-S bonds as covalent and, therefore, nonbreakable.

The native Cp Rd structure also has several partially exposed hydrophobic side chains, including those of V8, L41, and V44 (cf. Fig. 1). As inferred from our NMR data, these side chains undergo environmental changes upon increasing the temperature, which are most likely due to increased solvent exposure. It is possible that, above the temperature threshold indicated by ANS-binding data (50–60 °C), at least some of these residues become nearly fully solvent exposed and, as is often observed for other heat-treated proteins (Cairoli et al., 1994; Iametti et al., 1996), that they cluster themselves into discrete "hydrophobic patches" on the protein surface. These transitions are completed just prior to the onset of the likely more extensive modifications made evident by DSC.

All of the thermally induced structural modifications so far discussed are attributable to "loosening" of several intramolecular interactions, but are reversible upon lowering the temperature. While these modifications do not directly involve the metal site, they generally occur at lower temperatures in CdRd than in ZnRd. The larger Cd^{2+} ion may drive a "wedge" into the native structure, allowing for easier thermally induced opening than for the smaller Zn^{2+} ion, despite the inherently weaker M-SCys ligation of the latter. This size vs. thermal stability correlation also encompasses reduced FeRd. Based on the higher temperature onset of changes in the NMR spectrum, the intraprotein interactions are stronger for M = Fe^{2+} than for either Cd^{2+} or Zn^{2+}. The X-ray crystal structures of Cp Rds show 0.08 Å shorter M-SCys distances for M = Fe^{2+} vs. Zn^{2+} (Dauter et al., 1996). Thus, the smallest of the three

Table 2. *Temperature parameters of molecular events detected by various methods during progressive heating of Mrds* [a]

Technique	Molecular event		Metal ion in Rd			
			Fe^{3+}	Fe^{2+}	Cd^{2+}	Zn^{2+}
UV/Vis, chemical analysis	Metal release	T_m	83	69	ND[b]	ND
		T_{onset}	>60	>50	>80	>70
DSC	Overall protein solvation	T_m	52	None	72	94
ANS-binding	Exposure of hydrophobic regions	T_m	ND	ND	50	60
W37 fluorescence	Modifications of indole ring environment		ND	ND	PR[c]	PR
^{1}H-NMR	Modifications of W37 indole NH environment		ND	PR	PR	PR
	Exposure of W37 indole NH to solvent		ND	>80	70	80
	Change in the temperature dependence of I33 δCH_3 shift	ND	None	65	65	

[a] Temperatures are in °C.
[b] ND, not detectable.
[c] PR, progressive from ~25 to ~80 °C.

divalent $M(SCys)_4$ sites, i.e., $M = Fe^{2+}$, induces the strongest intraprotein interactions in Cp Rd.

The final, irreversible phase of thermally induced Rd unfolding could involve a structural modification of the $M(SCys)_4$ site, for which no direct evidence was detected. This hypothetical modification should greatly facilitate metal ion release, which occurs in the Cp Rds at significant rates only above ~80 °C. Our results indicate that metal ion release from Cp Zn and CdRd is dependent mostly on the inherent metal–sulfur bond strength. We previously proposed that protonation of the most solvent-exposed cysteinyl sulfur ligand (Cys42) is responsible for the acid-induced release of M^{2+} from Cp MRds (Bonomi et al., 1998). Thus, H^+ would compete with M^{2+} for the cysteinyl sulfur. Concomitant with metal ion release at high temperature, the residual apoprotein unfolds rapidly and completely in an irreversible process, as made evident by intrinsic W37 fluorescence spectra and far-UV CD.

The same general pattern of events depicted above for Zn and CdRd occurs upon heating reduced FeRd. However, some temperature-dependent features of the NMR spectra of reduced FeRd are different from those of Zn and CdRds. For example, changes in the positions of either the W37 indole NH or the I33 δCH_3 resonances were relatively limited, no sharp transitions in their temperature dependences were evident, and the W37 indole NH signal did not disappear completely even at 80 °C. Thus, the conformation of the hydrophobic core (including W37 and I33) of reduced FeRd apparently remains more compact than that of Zn and CdRd during heating. However, the weaker Fe^{2+}-SCys bonds result in loss of M^{2+} at a lower temperature, and this loss is rapidly followed by unfolding of the apoprotein. Indeed, the transition observed at 57 °C in the Arrhenius plot for iron release from reduced FeRd (Fig. 1S in Supplementary material in the Electronic Appendix), indicating a sudden change in the reaction pathway, coincides with the onset of thermal release of Fe^{2+} in temperature-ramp experiments (Fig. 4). This coincidence confirms the kinetic nature of the barrier to Fe^{2+} release concomitant with protein unfolding.

We have demonstrated that under anaerobic conditions Fe^{3+} is reduced by cysteine thiols upon thermal denaturation of oxidized Cp FeRd, and that the resulting Fe^{2+} is rapidly released. It is worth noting that, while release of iron from the protein during thermal denaturation of oxidized FeRds has often been assumed, it had not

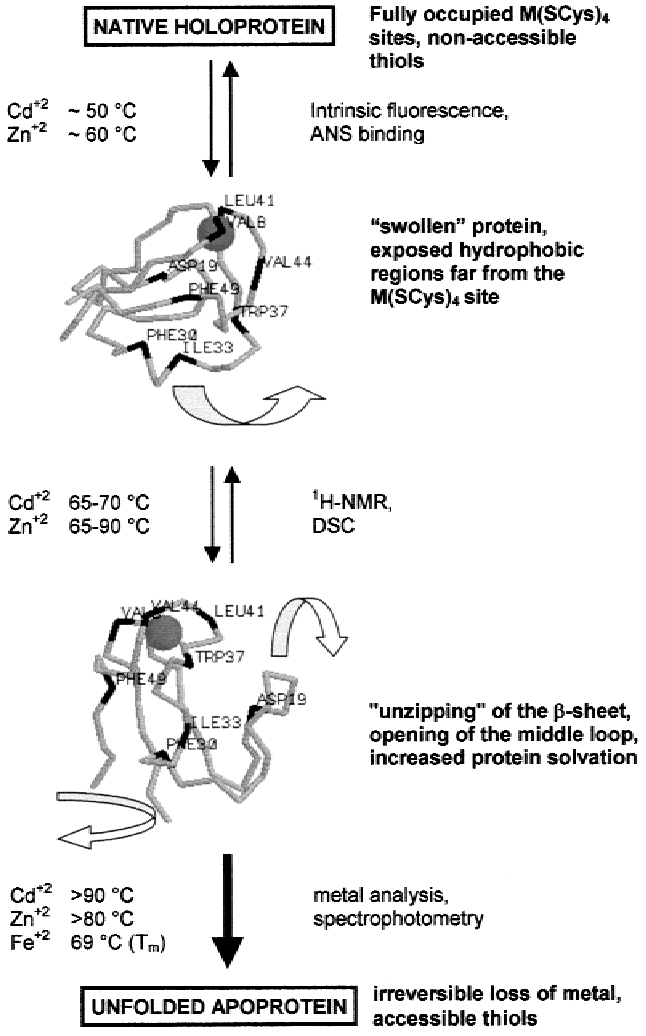

Scheme 1. A pictorial representation of the regions involved in structural modifications during exposure of CdRd and ZnRd at increasing temperature. The technique used for detecting individual steps and the temperature range in which they occur are given for each protein. Ribbon arrows indicate regions of the protein that are involved in each denaturation step.

heretofore been directly demonstrated. We suggest that inhibition of the aforementioned Fe^{3+}/thiolate redox chemistry by O_2 explains the higher activation barrier measured by Cavagnero et al. (1998a) for thermal denaturation of oxidized Cp FeRd in their stirred, aerobic solutions (213 kJ mol^{-1} between 60 and 80 °C vs. 70–72 kJ mol^{-1} measured in this study). The same inhibition would also explain the much longer times (several hours) required for loss of the UV-vis absorbance of oxidized Cp FeRd at 92 °C reported by Eidsness et al. (1997).

Nonnative $Fe^{3+}(SCys)_n$ species do not accumulate to any detectable extent during thermal denaturation under either aerobic or anaerobic conditions. This observation, coupled with the inhibition by O_2, suggests that reduction of Fe^{3+} occurs in the rate-determining step. Our [reactive thiol]/[released iron] stoichiometry for thermally denatured oxidized Cp FeRd (Table 1) indicates that reduction of each Fe^{3+} to Fe^{2+} is accompanied by oxidation of one thiol. Because no aggregation of the resulting apoRd was observed, the oxidation product cannot be an intermolecular disulfide. A solely intramolecular mechanism for this one-electron/two-electron iron/thiol redox chemistry is not obvious to us. Wampler and Neuhaus (1997) invoked an intermolecular autocatalytic mechanism to fit the thermal denaturation kinetics of oxidized FeRds, including that from Cp, in aerobic solutions. Under our anaerobic conditions the time course of thermally induced $Fe^{3+}(SCys)_n$ site destruction in Cp Rd was the same in either the presence or absence of the Fe^{2+} chelator, BPS. Therefore, iron released from the Rd does not appear to be a catalyst under our conditions. Interprotein interactions would then seem to be a viable alternative explanation for the iron/thiol redox stoichiometry observed during thermal denaturation of oxidized Cp FeRd.

The thermally prepared Cp apoRd does not show any residual secondary structure at room temperature after metal ion loss, even under anaerobic conditions. Conversely, the Cp apoRd prepared by TCA precipitation at room temperature retains a considerable degree of residual secondary structure at 25 °C. This last result appears to be in conflict with the results of Strop and Mayo (1999), who found that their cysteine–ligand mutated mesophilic apoRd contained no detectable secondary structure even at 1 °C. This apparent conflict likely stems at least in part from kinetically vs. thermodynamically controlled protein denaturation. We propose that incorporation of M^{2+} into Cp Rd optimizes a large number of interactions throughout the protein that together stabilize the native folded structure. This set of interactions plus the inherent stability of the $M(SCys)_4$ site would increase the thermodynamic stability of the native Cp MRd structure and also raise the activation barrier to thermal unfolding. Thus, once folded into its native structure, Cp Rd must have a significant activation barrier to complete unfolding, even when the metal ion is removed.

The published thermal unfolding studies of native Pf Rd have not resolved the kinetic versus thermodynamic contributions to its hyperthermostability. DSC experiments gave (irreversible) unfolding midpoint temperatures for Pf Fe^{2+} and Fe^{3+} Rds of 102 and 113 °C, respectively (Klump et al., 1994). Hydrogen exchange measurements led to an estimated T_m close to 200 °C for Pf ZnRd (Hiller et al., 1997). These temperatures are all significantly higher than the reversible T_m of 82 °C for the cysteine–ligand-mutated Pf apoRd (Strop & Mayo, 1999). Thermal denaturation of oxidized Pf FeRd in aerobic conditions between 60 and 80°C was only measurable at low pH (Cavagnero et al., 1998b), and, here again, was irreversible. Given our results showing much more rapid thermally induced loss of iron from Cp Fe^{2+} vs. Fe^{3+}Rd, a thermal denaturation study of reduced Pf FeRd, and Pf apoRd under anaerobic conditions near neutral pH would seem to be worthwhile.

The relative thermal instability of reduced Cp FeRd in vitro may have implications in vivo. FeRd, the biologically active form with $E_m = -55$ mV vs. NHE at room temperature, is likely to be predominantly reduced in the anaerobic and extremely reducing environment of *Clostridium pasteurianum*, which grows optimally at 37 °C. Extrapolating from the data in Figures 4 and 1S (see Supplementary material in the Electronic Appendix), the estimated half-life of native reduced Cp FeRd at 37 °C is ~30 h. This estimate applies only to "spontaneous" thermally induced iron loss and does not include the possibility of direct metal exchange or reinsertion. This analysis could imply a fairly rapid turnover of FeRd in vivo, for which there is currently no evidence. An alternative and perhaps more likely possibility is an in vivo system for actively inserting iron into the Rd apoprotein and/or for inhibiting its release. We have previously suggested that Zn^{2+}, which our results show can displace Fe^{2+} from Cp Rd, is sequestered from reduced FeRd in vivo (Bonomi et al., 1998).

Materials and methods

Proteins and analytical methods

A recombinant *C. pasteurianum* Rd obtained via overexpression in *E. coli* was used for all experiments. FeRd and ZnRd were obtained and purified as described elsewhere (Eidsness et al., 1992; Richie et al., 1996). CdRd was prepared from either Fe or ZnRd following a nondenaturing metal substitution procedure (Bonomi et al., 1998). Rd concentration was determined by using ϵ_{492} = 8,850 M^{-1} cm^{-1} for oxidized FeRd (Lovenberg & Walker, 1978), ϵ_{280} = 9,530 M^{-1} cm^{-1} for ZnRd (Eidsness et al., 1992; Richie et al., 1996), or ϵ_{280} = 10,560 M^{-1} cm^{-1} for CdRd (Bonomi et al., 1998). Iron was determined spectrophotometrically with bathophenanthroline sulfonate (BPS) in the presence of sodium dithionite after protein denaturation (Ljones & Burris, 1978), or, along with other metals, by inductively coupled plasma-atomic emission (ICP-AE) at the Chemical Analysis Laboratory, University of Georgia. Residual free thiols in the thermally treated proteins were measured spectrophotometrically by using Ellman's reagent (Ellman, 1959) in Tris buffer at pH 7.4.

Kinetics of metal release from Rd at fixed temperature

All manipulations were carried out anaerobically by working in either septum-capped vials or Schlenk-type flasks where air was replaced by high-purity Ar through several cycles of evacuation and refilling. Standard anaerobic techniques and gas-tight syringes were used for sample handling. Aliquots (0.1 mL) of a stock Rd solution (0.08–0.1 mM Rd in 50 mM Tris-HCl, pH 7.4) were diluted 10-fold with the same buffer, and heated in a thermostatted water bath or, in the case of the reduced FeRd, in a Peltier-equipped spectrophotometer cell holder. After the required time, samples were exhaustively buffer-exchanged in Centricon® devices at room temperature to remove any unbound metal. Buffer exchange was carried out aerobically. The amount of residual protein-bound metal was then determined as indicated in the above paragraph. In experiments involving FeRd, the time course of metal release was also followed by monitoring the loss of absorbance at 492 nm (for the oxidized protein) or the increase in absorbance at 535 nm due to the forma-

tion of the red Fe(II)BPS complex in heated mixtures of the protein and BPS. The experiments involving BPS were performed on both the oxidized and the reduced form of FeRd. In the latter case, a diluted FeRd solution was made anaerobic and reduced by addition of sodium dithionite to a final concentration of 2–5 mM. BPS was then added anaerobically from a 10 mM stock solution to a final concentration of 0.1–0.2 mM. All reported pseudo-first-order rate constants were calculated from $\ln[(A_t - A_\infty/(A_0 - A_\infty)]$ vs. time plots, which were linear for at least two half-lives.

Temperature-ramp experiments

Time-progressive heating of protein solutions was performed in computer-controlled, Peltier-driven cell holders, fitting a spectrophotometer or a spectrofluorometer. Typically, spectroscopic signals were monitored continuously while applying the following temperature gradient: 20 °C for 5 min; from 20 to 100 °C in 160 min (heating rate: 0.5 °C/min); 100 °C for 5 min. To assess the extent of reversibility, the sample was cooled to 20 °C over an 8 min period (cooling rate, 10 °C/min). In all these experiments, the proteins were 8–10 μM in 50 mM Tris-HCl, pH 7.4. In experiments aimed at monitoring the exposure of hydrophobic surfaces, 1–8 anilinonaphthalenesulfonate (ANS) was added to the proteins from a 20 mM stock solution in buffer to a final concentration of 0.1 mM. Release of iron from FeRd was monitored spectrophotometrically as reported above for kinetic studies at fixed temperature. For the determination of midpoint transition temperatures (T_m), the temperature ramp curves were corrected for delay effects (Riva & Schiraldi, 1993) by using an home-written program.

Spectroscopy

Electronic absorption spectra were recorded on Shimadzu (UV2101PC) or Perkin-Elmer scanning spectrophotometers using anaerobic 1 cm pathlength cells. All spectrofluorimetric measurements were performed in a LS-50 Perkin-Elmer instrument, by using anaerobic 1 mL cells. Far-UV CD spectra were taken by using 1 mm pathlength cells in a JASCO J-500 instrument, and analyzed by JASCO software. ^{1}H NMR experiments were performed on a Bruker AMX600 spectrometer operating at 600 MHz for the ^{1}H nucleus, in H_2O/D_2O 90:10 v/v solutions containing 0.4–0.5 mM MRd in ~5 mM Tris/HCl, pH 7.4. In variable temperature experiments, the protein was heated progressively in 5 °C steps (heating rate ~1 °C/min) between 25 and 80 °C. About 15 min were allowed for thermal equilibration of the sample, and acquisition of a single spectrum took 15–20 min at each preset temperature. Chemical shifts were referred to the methyl resonance of 3-(trimethylsilyl)propanesulfonate, as an external reference. This reference was used to calibrate the residual water signal (at 4.76 ppm, 25 °C), then used as a reference in spectra taken at different temperatures. Off-line data processing was performed using either the UXNMR software (v. 950901) installed on the NMR spectrometer, or XWINNMR (Bruker Spectrospin, v. 1.1) installed on a Silicon Graphics Indy workstation.

Differential scanning calorimetry

Calorimetric measurements on 0.4–0.5 mM protein solutions in 50 mM Tris-HCl, pH 7.4 were carried out on a third-generation Setaram Micro-DSC apparatus. All samples were prepared anaerobically and were transferred to the calorimetric cell under an Ar atmosphere in a glove box. Scan rate was 0.5 K/min. The data were analyzed by using the THESEUS software package by the method of Barone et al. (1992). The observable quantity is the excess molar heat capacity $\langle Cp(T)\rangle$, i.e., the apparent molar heat capacity $Cp(T)$ of the sample per mol of protein, referred to the molar heat capacity of the "native state," $Cp_N(T)$, at each temperature. The latter is obtained according to the Freire and Biltonen procedure (Freire & Biltonen, 1978), by the linear regression of $Cp(T)$ in the pre-denaturation region. At least two separate experimental runs were performed for each sample.

Acknowledgments

This work was supported in part by grants from the Ministry for University and Scientific and Technologic Research, and the National Research Council of Italy (MURST, CNR, Rome, Italy, to F.B.) and the National Institutes of Health (GM50736, to D.M.K.). Travel support was available through a NATO Collaborative Research Grant (CRG 971030, to F.B. and D.M.K.).

References

Ayhan M, Xiao Z, Lavery MJ, Hamer AM, Nugent KW, Scrofani SDB, Guss M, Wedd AG. 1996. The rubredoxin from *Clostridium pasteurianum*: Mutation of the conserved glycine residues 10 and 43 to alanine and valine. *Inorg Chem 35*:5902–5911.

Barone G, Del Vecchio P, Fessas D, Giancola C, Graziano G. 1992. THESEUS: A new software package for the handling and analysis of thermal denaturation data of biological macromolecules. *J Thermal Anal 38*:2779–2790.

Barone G, Del Vecchio P, Fessas D, Giancola C, Graziano G, Riccio A. 1994. Thermal behaviour of three ribonucleases. In: Russo N, Anastassopoulou J, Barone G, eds. *Chemistry and properties of biomolecular systems.* Dordrecht: Kluwer. pp 49–65.

Bau R, Rees DC, Kurtz DM Jr, Scott RA, Huang H, Adams MWW, Eidsness MK. 1998. Crystal structure of rubredoxin from *Pyrococcus furiosus* at 0.95 Å resolution, and the structures of N-terminal methionine and formylmethionine variants of Pf Rd. Contributions of N-terminal interactions to thermostability. *J Biol Inorg Chem 3*:484–493.

Bertini I, Kurtz DM Jr, Eidsness MK, Liu G, Luchinat C, Rosato A, Scott RA. 1998. Solution structure of reduced *Clostridium pasteurianum* rubredoxin. *J Biol Inorg Chem 3*:401–410.

Blake PR, Park JB, Bryant FO, Aono S, Magnuson JK, Eccleston E, Howard JB, Summers MF, Adams MWW. 1991. Determinants of protein hyperthermostability: Purification and amino acid sequence of rubredoxin from the hyperthermophilic archaebacterium *Pyrococcus furiosus* and secondary structure of the zinc adduct by NMR. *Biochemistry 30*:10885–10895.

Bonomi F, Iametti S, Kurtz DM Jr, Ragg E, Richie KA. 1998. Direct metal ion substitution at the $[M(SCys)_4]^{2-}$ site of rubredoxin. *J Biol Inorg Chem 3*:595–605.

Brouwer M. 1996. Role of metallothionen in intracellular metal metabolism and in activation of copper- and zinc-dependent proteins. In: Hausinger RP, Eichhorn GH, Marzilli LP, eds. *Mechanisms of metallocenter assembly.* New York: VCH. pp 235–260.

Cairoli S, Iametti S, Bonomi F. 1994. Reversible and irreversible modifications of betalactoglobulin upon exposure to heat. *J Protein Chem 13*:347–354.

Cavagnero S, Debe DA, Zhou ZH, Adams MWW, Chan SI. 1998a. Kinetic role of electrostatic interactions in the unfolding of hyperthermophilic and mesophilic rubredoxins. *Biochemistry 37*:3369–3376.

Cavagnero S, Zhou ZH, Adams MWW, Chan SI. 1998b. Unfolding mechanism of rubredoxin from *Pyrococcus furiosus*. *Biochemistry 37*:3377–3385.

Dauter Z, Wilson KS, Sieker LC, Moulis JM, Meyer J. 1996. Zinc- and iron-rubredoxins from *Clostridium pasteurianum* at atomic resolution: A high-precision model of a ZnS_4 coordination unit in a protein. *Proc Natl Acad Sci USA 93*:8836–8840.

Day MW, Hsu BT, Joshua-Tor L, Park JB, Zhou ZH, Adams MWW, Rees DC. 1992. X-ray crystal structures of the oxidized and reduced forms of the rubredoxin from the marine hyperthermophilic archaebacterium *Pyrococcus furiosus*. *Protein Sci 1*:1494–1507.

Eidsness MK, Richie KA, Burden AE, Kurtz DM Jr, Scott RA. 1997. Dissecting contributions to the thermostability of *Pyrococcus furiosus* rubredoxin: Beta-sheet chimeras. *Biochemistry 36*:10406–10413.

Eidsness MK, O'Dell SE, Kurtz DM Jr, Robson RL, Scott RA. 1992. Expression of a synthetic gene coding for the amino acid sequence of *Clostridium pasteurianum* rubredoxin. *Protein Eng 5*:367–371.

Ellman GL. 1959. Tissue sulfhydryl groups. *Arch Biochem Biophys 82*:70–77.
Freire E, Biltonen RL. 1978. Statistical mechanical deconvolution of thermal transitions in macromolecules. I. Theory and application to homogeneous systems. *Biopolymers 17*:463–479.
Gomes CM, Silva G, Oliveira S, LeGall J, Liu MY, Xavier AV, Rodrigues-Pousada C, Teixeira M. 1997. Studies on the redox centers of the terminal oxidase from *Desulfovibrio gigas* and evidence for its interaction with rubredoxin. *J Biol Chem 272*:22502–22508.
Hausinger RP, Eichhorn GH, Marzilli LP. 1996. General principles and mechanisms of metallocenter assembly. In: *Mechanisms of metallocenter assembly.* New York: VCH. pp 1–18.
Hiller R, Zhou ZH, Adams MWW, Englander SW. 1997. Stability and dynamics in a hyperthermophilic protein with melting temperature close to 200 °C. *Proc Natl Acad Sci USA 94*:11329–11332.
Iametti S, De Gregori B, Vecchio G, Bonomi F. 1996. Modifications occur at different structural levels during the heat denaturation of betalactoglobulin. *Eur J Biochem 237*:106–112.
Iametti S, Scaglioni L, Mazzini S, Vecchio G, Bonomi F. 1998. Structural features and reversible association of different quaternary structures of *β*-lactoglobulin. *J Agric Food Chem 46*:2159–2166.
Klump HH, Adams MWW, Robb FT. 1994. Life in the pressure cooker: Thermal unfolding of proteins from hyperthermophiles. *Pure Appl Chem 66*: 485–489.
Lazaridis T, Lee I, Karplus M. 1997. Dynamics and unfolding pathways of a hyperthermophilic and a mesophilic rubredoxin. *Protein Sci 6*:2589–2605.
Ljones T, Burris RH. 1978. Nitrogenase: The reaction between iron protein and bathophenanthroline disulfonate as a probe for interactions with MgATP. *Biochemistry 17*:866–1872.
Lovenberg W, Walker MN. 1978. Rubredoxin. *Methods Enzymol 53*:340–346.
Pountney DL, Vasak M. 1992. Spectroscopic studies on metal distribution in Co(II)/Zn(II) mixed-metal clusters in rabbit liver metallothionein 2. *Eur J Biochem 209*:335–341.
Privalov PL. 1979. Stability of proteins. Small globular proteins. *Adv Protein Chem 33*:167–241.
Privalov PL, Gill SJ. 1989. The hydrophobic effect: A reappraisal. *Pure Appl Chem 61*:1097–1104.
Privalov PL, Makhatadze GI. 1990. Heat capacity of proteins II. Partial molar heat capacity of the unfolded polypeptide chain of proteins: Protein unfolding effects. *J Mol Biol 213*:385–391.
Privalov PL, Makhatadze GI. 1992. Contribution of hydration and non-covalent interactions to the heat capacity effect on protein unfolding. *J Mol Biol 224*:715–723.
Privalov PL, Makhatadze GI. 1993. Hydration effects at protein unfolding. II. The entropy and Gibbs energy of hydration. *J Mol Biol 232*:660–679.
Ptitsyn OB. 1992. The molten globule state. In: Creighton TE, ed. *Protein folding.* New York: Freeman. pp 243–300.
Richie KA, Teng Q, Elkin CJ, Kurtz DM Jr. 1996. 2D ^{1}H and 3D ^{1}H-^{15}N NMR of zinc rubredoxins: Contributions of the beta-sheet to thermostability. *Protein Sci 5*:883–894.
Riva M, Schiraldi A. 1993. Kinetic parametrization of transitions and reactions in food systems from isothermal and non-isothermal DSC traces. *Thermochim Acta 220*:117–130.
Sayle RA, Milner-White EJ. 1995. RASMOL: Biomolecular graphics for all. *Trends Biochem Sci 20*:374–376.
Strop P, Mayo SL. 1999. Rubredoxin variant folds without iron. *J Am Chem Soc 121*:2341–2345.
Sturtevant JM. 1977. Heat capacity and entropy changes in processes involving proteins. *Proc Natl Acad Sci USA 74*:2236–2240.
Wampler JE, Neuhaus EB. 1997. A model for the unusual kinetics of thermal denaturation of rubredoxin. *J Prot Chem 16*:721–732.
Werth MT, Johnson MK. 1990. Magnetic circular dichroism and electron paramagnetic resonance studies of iron(II)-metallothionein. *Biochemistry 28*: 3982–3988.